Germanium Nanowire Growth Below the Eutectic Temperature
S. Kodambaka, *et al.*
Science **316**, 729 (2007);
DOI: 10.1126/science.1139105

References and Notes

1. V. Giovannetti, S. Lloyd, L. Maccone, *Science* **306**, 1330 (2004).
2. V. Meyer *et al.*, *Phys. Rev. Lett.* **86**, 5870 (2001).
3. D. Leibfried *et al.*, *Nature* **438**, 639 (2005).
4. C. F. Roos, M. Chwalla, K. Kim, M. Riebe, R. Blatt, *Nature* **443**, 316 (2006).
5. A. Widera *et al.*, *Phys. Rev. Lett.* **92**, 160406 (2004).
6. J. M. Geremia, J. K. Stockton, H. Mabuchi, *Science* **304**, 270 (2004).
7. J. Jacobson, G. Björk, I. Chuang, Y. Yamamoto, *Phys. Rev. Lett.* **74**, 4835 (1995).
8. M. W. Mitchell, J. S. Lundeen, A. M. Steinberg, *Nature* **429**, 161 (2004).
9. P. Walther *et al.*, *Nature* **429**, 158 (2004).
10. F. W. Sun, B. H. Liu, Y. F. Huang, Z. Y. Ou, G. C. Guo, quant-ph/0512212 (2005).
11. K. J. Resch *et al.*, quant-ph/0511214 (2005).
12. J. G. Rarity *et al.*, *Phys. Rev. Lett.* **65**, 1348 (1990).
13. A. Kuzmich, L. Mandel, *Quant. Semiclass. Opt.* **10**, 493 (1998).
14. E. J. S. Fonseca, C. H. Monken, S. Pádua, *Phys. Rev. Lett.* **82**, 2868 (1999).
15. K. Edamatsu, R. Shimizu, T. Itoh, *Phys. Rev. Lett.* **89**, 213601 (2002).
16. H. S. Eisenberg, J. F. Hodelin, G. Khoury, D. Bouwmeester, *Phys. Rev. Lett.* **94**, 090502 (2005).
17. A. N. Boto *et al.*, *Phys. Rev. Lett.* **85**, 2733 (2000).
18. M. D'Angelo, M. V. Chekhova, Y. Shih, *Phys. Rev. Lett.* **87**, 013602 (2001).
19. M. J. Holland, K. Burnett, *Phys. Rev. Lett.* **71**, 1355 (1993).
20. J. J. Bollinger, W. M. Itano, D. J. Wineland, D. J. Heinzen, *Phys. Rev. A.* **54,** R4649 (1996).
21. Z. Y. Ou, *Phys. Rev. A.* **55**, 2598 (1997).
22. J. P. Dowling, *Phys. Rev. A.* **57**, 4736 (1998).
23. R. A. Campos, C. C. Gerry, A. Benmoussa, *Phys. Rev. A.* **68**, 023810 (2003).
24. The visibility $V \equiv (max - min)/(max + min)$, where *max* and *min* are the extreme values of the sinusoidal multiphoton interference fringe; $0 \leq V \leq 1$.
25. C. K. Hong, Z. Y. Ou, L. Mandel, *Phys. Rev. Lett.* **59**, 2044 (1987).
26. R. A. Campos, B. E. A. Saleh, M. C. Teich, *Phys. Rev. A.* **40**, 1371 (1989).
27. Z. Y. Ou, J.-K. Rhee, L. J. Wang, *Phys. Rev. Lett.* **83**, 959 (1999).
28. O. Steuernagel, *Phys. Rev. A.* **65**, 033820 (2002).
29. K. Tsujino, H. F. Hofmann, S. Takeuchi, K. Sasaki, *Phys. Rev. Lett.* **92**, 153602 (2004).
30. Z. Y. Ou, *Phys. Rev. A.* **72**, 053814 (2005).
31. G. Y. Xiang *et al.*, *Phys. Rev. Lett.* **97**, 023604 (2006).
32. S. Takeuchi, J. Kim, Y. Yamamoto, H. H. Hogue, *Appl. Phys. Lett.* **74**, 1063 (1999).

33. We thank H. F. Hofmann, K. J. Pregnell, G. J. Pryde, J. G. Rarity, K. J. Resch, and A. G. White for helpful discussions. This work was supported by the Japan Science and Technology Agency (JST), Ministry of Internal affairs and Communication (MIC), Japan Society for the Promotion of Science (JSPS), 21st Century Centers of Excellence program, Special Coordination Funds for Promoting Science and Technology, and the Daiwa Anglo-Japanese Foundation. J.L.O'B. was supported by an Australian Academy of Science–JSPS Fellowship.

Supporting Online Material

www.sciencemag.org/cgi/content/full/316/5825/726/DC1
SOM Text

27 November 2006; accepted 18 January 2007
10.1126/science.1138007

Germanium Nanowire Growth Below the Eutectic Temperature

S. Kodambaka,* J. Tersoff, M. C. Reuter, F. M. Ross†

Nanowires are conventionally assumed to grow via the vapor-liquid-solid process, in which material from the vapor is incorporated into the growing nanowire via a liquid catalyst, commonly a low–melting point eutectic alloy. However, nanowires have been observed to grow below the eutectic temperature, and the state of the catalyst remains controversial. Using in situ microscopy, we showed that, for the classic Ge/Au system, nanowire growth can occur below the eutectic temperature with either liquid or solid catalysts at the same temperature. We found, unexpectedly, that the catalyst state depends on the growth pressure and thermal history. We suggest that these phenomena may be due to kinetic enrichment of the eutectic alloy composition and expect these results to be relevant for other nanowire systems.

Self-assembled semiconducting nanowires are promising candidates for applications in nanoelectronics, optoelectronics, and sensors (*1-4*). Progress in designing more complex structures, such as branched or compositionally modulated wires, requires a clear understanding of nanowire growth mechanisms. Nanowires are conventionally assumed to grow via the vapor-liquid-solid (VLS) process (*5*), in which material from the vapor is incorporated via a liquid catalyst, commonly a low–melting point eutectic alloy. Yet, in many important semiconductor/catalyst systems [e.g., Si/Al (*6*), Si/Cu (*7*), Si/Ti (*8*), Ge/Au (*9–14*), GaAs/Au (*15–18*), and InAs/Au (*15*, *19*, *20*)], nanowire growth can occur below the bulk eutectic temperature T_e. The state of the catalyst remains controversial, but it is important because it is expected to influence growth kinetics, orientation, and morphology. Most importantly, because interface formation in heterostructure nanowires depends on diffusive processes through the catalyst, the catalyst state is also expected to determine interface sharpness. Post-growth analyses have yielded contradictory conclusions regarding the catalyst state; speculations include the existence of a liquid catalyst below T_e (*17*) stabilized by nanoscale size effects (*20*) and growth via a vapor-solid-solid (VSS) mechanism (*8*, *9*) with a solid catalyst. Using in situ microscopy, we show for the classic Ge/Au system that catalysts can be either liquid or solid below T_e, depending on thermal history. Moreover, nanowires grow in both cases (i.e., both VLS and VSS processes occur), although at different rates. Unexpectedly, the catalyst state depends on Ge_2H_6 pressure as well as temperature: The supersaturation of Ge in the alloy caused by the growth process appears to be essential in stabilizing the liquid below T_e.

Ge wire growth experiments were carried out in a multichamber ultrahigh vacuum system (base pressure, 2×10^{-10} Torr) based around a transmission electron microscope (TEM) with in situ physical and chemical vapor deposition facilities (*21*). Si(111) substrates were loaded into the TEM and cleaned by heating resistively to 1250°C. After cooling, a 2- to 3-nm-thick Au film was evaporated onto the polished surface. The sample was vacuum annealed at ~400°C for 5 min, allowing the Au film to agglomerate, and wire growth was initiated by cooling to the growth temperature and leaking in a gas mixture composed of 20% Ge_2H_6 and 80% He. The temperature versus heating current curve

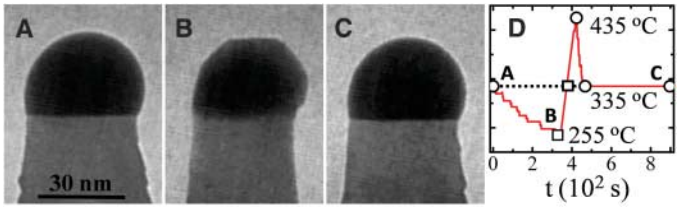

Fig. 1. (**A** to **C**) Bright-field TEM images showing the solid-to-liquid and liquid-to-solid transitions in a Au-Ge catalyst particle at the tip of a Ge wire during cooling and heating, acquired at times t = 0 s (A), 328 s (B), and 897 s (C), respectively. (**D**) The sample temperature versus time and catalyst state (open circle, liquid; open square, solid) are shown. The letters "A," "B," and "C" refer to the images in the respective panels in the figure. We initiated wire growth by first heating to above T_e (361°C) and then cooling to T_0 ~335°C while maintaining a constant digermane pressure of 1.6×10^{-6} Torr. After a period of growth, the sample temperature is reduced to 255°C, at which point the catalyst solidifies (B). On heating, the catalyst does not melt until 435°C, after which the temperature is returned to 335°C (C).

IBM T. J. Watson Research Center, Yorktown Heights, NY 10598, USA.

*Present address: Materials Science Department, University of California Los Angeles, Los Angeles, CA 90024, USA.
†To whom correspondence should be addressed. E-mail: fmross@us.ibm.com

was calibrated post-growth for each specimen, with the use of both pyrometry and a thermocouple mounted on the specimen's back surface. This procedure allows us to estimate the substrate temperature T_0 to within 50 K, and relative changes in temperature in a single experiment can be determined more accurately.

In the pressure range accessible in our in situ system (Ge_2H_6 pressures between 10^{-7} and 10^{-5} Torr), we typically observe sustained growth of ⟨111⟩-oriented Ge wires at temperatures in the 250° to 400°C range. Under these conditions, most wires grow perpendicular to the substrate and are imaged with the electron beam perpendicular to the wire axis (*21*). Bright-field and dark-field imaging show that the wires are epitaxial, single-crystal, and are bounded by smooth sidewalls. Furthermore, by the acquisition of video images at 30 frames per second, growth kinetics for individual wires can be measured.

Figure 1 shows a series of bright-field images of a single Ge nanowire during growth at constant Ge_2H_6 pressure as the temperature is varied. The image in Fig. 1A, at T_0 = 335°C, is typical of wire growth by the VLS process. The tip is composed of a Au-Ge eutectic droplet with a smoothly curved surface. Upon cooling to a lower temperature, in this case ~106 K below T_e = 361°C, we observe abrupt solidification of the droplet, as indicated both by the facetted surface (Fig. 1B) and by the dark-field contrast (fig. S1). We also see an abrupt increase (within a single video frame) in the length of the wire, indicating that Ge is coming out of solution as the droplet solidifies, as expected. On increasing the temperature again to the original value T_0, we find that the solid particle does not transform back into a liquid. Reestablishing the liquid phase requires a temperature well above T_0 (Fig. 1C). However, once the liquid has re-formed, upon cooling to T_0, we return to VLS growth with the same growth rate as initially observed. This hysteresis in the solid-liquid phase transformation is seen in all our Ge growth experiments and for wires with a range of diameters (20 to 140 nm).

Hysteresis with temperature is normal for first-order phase transitions and is likely to be exacerbated at the nanoscale (*22*, *23*). Thus, it is not surprising that hysteresis is so clearly visible in these experiments. However, close inspection of video images such as those in Fig. 1 shows that the wires continue to grow even after the catalyst particle has solidified.

This VSS growth process is illustrated in Fig. 2. Figure 2A shows a Ge wire at three successive times during VLS growth at 340°C and 4.8×10^{-6} Torr Ge_2H_6. In this experiment, we initiated wire growth ~78 min before acquiring the first image at time t = 0. After cooling the specimen to solidify the catalysts and then reheating to 340°C, all at constant Ge_2H_6 pressure, we observed wire growth to continue with solid catalysts (Fig. 2B). Measurements made on several wires show that VSS growth is 10 to 100 times slower than VLS growth at the same Ge_2H_6 pressure and temperature, presumably as a result of weaker surface reactivity and/or lower diffusivity through the solid. We can obtain prolonged wire growth by either VLS or VSS mechanisms at identical temperatures and Ge_2H_6 pressures, depending (via hysteresis) on the thermal history of the sample. We have actually seen VLS and VSS growth occurring simultaneously on neighboring wires in some instances. All the wires, irrespective of the growth mode, are crystalline, and the only obvious difference between the growth modes is that the VSS process yields more tapered wires owing to their relatively slower growth rates. This demonstration of dual growth modes may be relevant to the controversy regarding the role of VSS and VLS growth in other systems (*6*, *16*–*20*).

We also find that Ge_2H_6 pressure can be as important as temperature in controlling the growth mode. Indeed, a substantial Ge_2H_6 pressure appears to be essential for stabilizing the liquid state below T_e. Whenever the Ge_2H_6 pressure is reduced during VLS growth, we find that the catalyst droplets solidify. The fact that the droplets can solidify confirms that the temperature is definitely below T_e, independent of any uncertainties in temperature calibration.

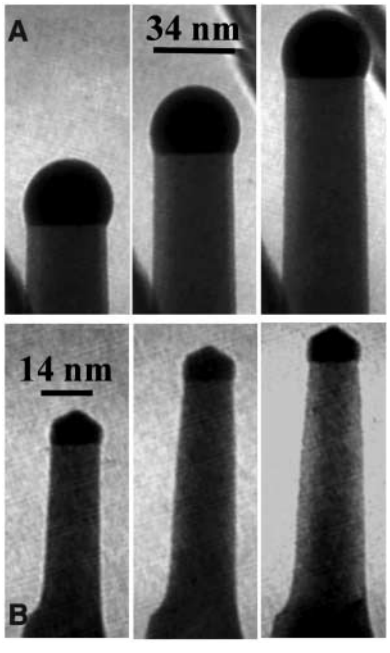

Fig. 2. (**A**) Series of images of a single Ge wire acquired at times t = 0, 309, and 618 s (from left to right, respectively) during growth by the VLS mechanism at 340°C and 4.6×10^{-6} Torr Ge_2H_6. The background features act as markers, showing a growth rate of 9.9×10^{-2} nm/s. (**B**) Another image series for a second wire growing at the same temperature and pressure but with a solid catalyst at t = 0, 1340, and 1824 s (from left to right, respectively). The growth rate for this VSS mode is 1.3×10^{-2} nm/s.

The role of Ge_2H_6 pressure (i.e., growth rate) in the nanowire growth mode is illustrated in Fig. 3A. The first image (Fig. 3A, left panel) shows two Ge wires after 3 hours and 24 min of stable VLS growth at 4.8×10^{-6} Torr. The Ge_2H_6 pressure was then reduced to 8.6×10^{-7} Torr while a constant temperature was maintained. Within 106 s, the droplet on the narrower wire abruptly solidifies (Fig. 3A, middle panel), while the droplet on the wider wire solidifies later (Fig. 3A, right panel). This behavior has been verified for larger samples of wires. Figure 3B shows the catalyst state versus wire diameter in one experiment at an intermediate time. The reduction in Ge_2H_6 pressure causes all the droplets to solidify, although there can be a time delay of several minutes, with the smaller droplets solidifying earlier. (The exact time delay between smaller and larger droplets depends on the growth history and in some cases were as long as 20 to 60 min.

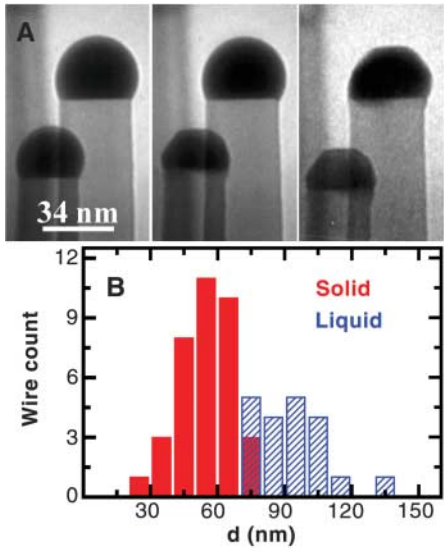

Fig. 3. (**A**) Representative bright-field TEM image series showing the solidification of Au-Ge catalysts on top of two Ge wires (29 and 34 nm in diameter) when the pressure is reduced during growth at constant temperature. We carried out wire growth at 350°C using 4.8×10^{-6} Torr Ge_2H_6 for 3 hours 24 min (left panel), after which we reduced the pressure to 8.6×10^{-7} Torr. After 106 s, the catalyst in the narrower wire solidified (middle panel) and, after a further 283 s, the catalyst on the wider wire solidified (right panel). (**B**) Histogram showing the diameter dependence of the catalyst state at a fixed time after reducing the pressure. Wire growth is carried out at 8×10^{-6} Torr and 355°C for 2 hours. At this time, the Ge_2H_6 pressure is reduced to 5×10^{-7} Torr; no change is observed after 15 min. The Ge_2H_6 supply is then switched off (leaving a background pressure of 6×10^{-10} Torr), and the state of the catalysts on 56 wires is recorded after 14 min. Wires with diameters (d) less than 70 nm have solid tips, whereas the tips of those with diameters larger than 80 nm are still liquid.

Au-catalyzed growth of Ge wires below T_e is generally assumed to occur by a VLS process (i.e., via a liquid catalyst) (*9, 11–14*). The existence of a liquid alloy phase below T_e has been attributed to nanoscale size effects and, in particular, to a lowering of the droplet eutectic temperature to below T_e by the Gibbs-Thomson effect (*14*). This picture naturally leads to a dependence on size but does not directly involve growth pressure or growth rate.

Nevertheless, the fact that Ge_2H_6 pressure affects the droplet state does not in itself rule out a Gibbs-Thomson effect, because pressure could influence surface energies (for example, through changes in hydrogen coverage). In situ imaging allows us to examine the effect of Ge_2H_6 pressure on surface energies. Any change in surface energies will modify the force balance at the triple phase line and, hence, the steady-state droplet shape and wire diameter (*24*). We therefore measured the shapes of droplets during wire growth as a function of Ge_2H_6 pressure. Figure 4 is a typical plot of droplet heights and base diameters for an individual wire, as the pressure is varied repeatedly between higher and lower values. Although the changes are small, we find consistently that when the Ge_2H_6 pressure is decreased, the droplet height decreases while the droplet diameter increases. Clearly, the droplet shape is varying with Ge_2H_6 pressure, suggesting that there are observable changes in surface energy with pressure.

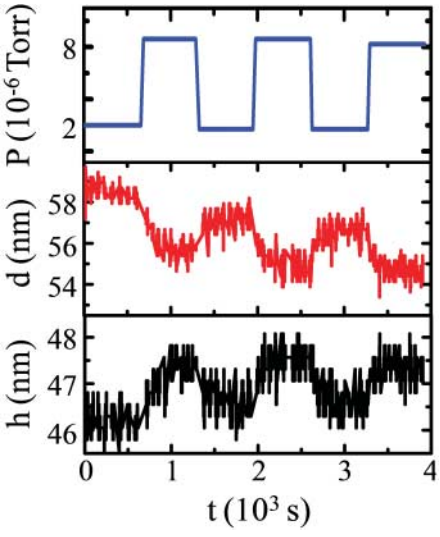

Fig. 4. The shape of a single droplet on a 59-nm-diameter Ge wire as a function of pressure, at a constant temperature of 355°C. Ge_2H_6 pressure P (blue curve), droplet base diameter or nanowire diameter d (red curve), and droplet height h (black curve) are plotted versus deposition time t as P is cycled repeatedly between 1.9×10^{-6} and 8.4×10^{-6} Torr. The measurements are taken from a video sequence of bright-field images, with h defined as the maximum normal distance from the drop boundary to the solid-liquid interface and with d defined as the width of the solid-liquid interface.

If the Gibbs-Thomson effect were stabilizing liquid-phase catalysts at temperatures below T_e, we would expect that droplets on narrower wires would be more resistant to solidification. In contrast, we observe that smaller droplets solidify sooner than larger ones, as in Fig. 3. This diameter dependence of solidification suggests that the principal cause of VLS growth below T_e is probably not the Gibbs-Thomson effect or any direct effect of small size.

Why then does the liquid phase persist below T_e? Some degree of undercooling is normal and may become more extreme at the nanoscale, but that does not explain the observed dependence on Ge_2H_6 pressure and diameter. We can rule out a dependence of the wire tip temperature on the wire diameter [via thermal conductivity (*25*)] or on the Ge_2H_6 pressure [via the heat of reaction (*9*)]: For wires with lengths <2 μm and for low pressures (10^{-7} to 10^{-5} Torr), both of which are typical in our experiments, we do not expect any appreciable variation in the tip temperature from these effects (*26*, *27*). Electron beam–induced temperature changes, if any, are small and are about the same for all wires being imaged simultaneously; hence, such changes should not affect the diameter dependence.

We suggest instead that the liquid phase may be effectively stabilized against solidification by Ge supersaturation, which arises from the growth process. Solidification requires some undercooling to overcome the nucleation barrier for a new phase. Here, crystalline Ge is already present. The key step for solidification is nucleation of a solid Au particle, and this step controls the degree of undercooling. Once Au nucleates, the liquid solidifies abruptly, with Ge coming out of solution and incorporating into the wire within a single video frame, as discussed earlier with reference to Fig. 1. Thus, the question to be addressed is why Au nucleation depends on Ge_2H_6 pressure.

By analogy with Si nanowire growth, we expect that the rate of dissociative adsorption of Ge_2H_6 at the droplet surface rises linearly with Ge_2H_6 pressure (*21*). Then, the supersaturation of Ge in the droplet must rise until the rate of incorporation from the liquid into the wire equals the rate of arrival of Ge from the vapor. However, the liquid-solid interface is a nanoscale (111) facet, so incorporation requires continuous nucleation of steps, which is difficult because of the small facet area (*28*) and the high step energy expected for (111). Therefore, even a modest growth rate in this system may require an anomalously large supersaturation.

Such a Ge supersaturation inhibits nucleation of solid Au. This can be seen by referring to the phase diagram (*29*) in Fig. 5, where the "V" shape of the liquidus arises as follows. At a temperature T, solid Au is unstable in the presence of a liquid that is more Ge-rich than a composition $c_{Au}(T)$. Similarly, solid Ge is unstable with a liquid that is more Au-rich than $c_{Ge}(T)$. Above their crossing point at T_e, these lines correspond to the liquidus, defining a region where neither solid is stable. As discussed above, for our growth conditions, solidification occurs by nucleation of solid Au; apparently, nucleation of solid Ge in the liquid is kinetically excluded. Therefore, solidification can only occur in the region where solid Au is stable, below the curve $c_{Au}(T)$ shown in green in Fig. 5. Under Ge-rich conditions, this curve goes below T_e (dashed portion of green line). (We also expect some undercooling with respect to this curve, but we do not speculate about its magnitude.)

This mechanism could also explain why narrower wires solidify first. When the Ge_2H_6 pressure is lowered, the supersaturation begins to decrease as excess Ge is incorporated into the wire, either at the growth facet or by diffusing to the sidewall (*30*). This Ge loss occurs at a rate that scales with cross-sectional area or circumference of the wire, whereas the amount of excess Ge scales with droplet volume, so the time scale for the loss of supersaturation increases with increasing wire diameter, explaining the observed trend.

The most speculative point is whether the Ge supersaturation can be quantitatively large enough to account for the observations. We estimate that a 1% increase in Ge concentration

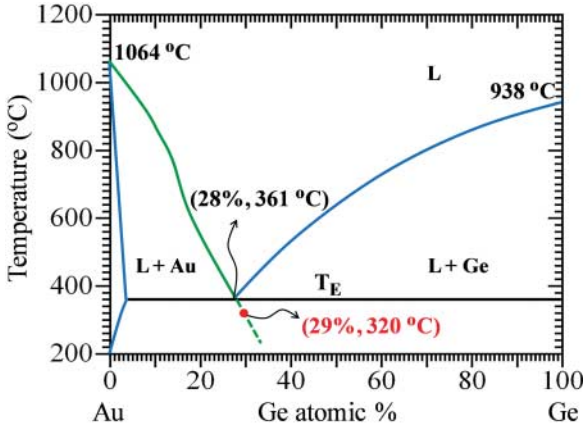

Fig. 5. Au-Ge binary alloy phase diagram [after (*29*)]. The solid green and blue curves are the Au and Ge liquidus lines, respectively. The dashed green curve is the extension of the Au liquidus line below T_e; Au nucleation cannot occur above this line. A 1% increase in Ge supersaturation in the liquid phase results in a ~40 K drop in the solid Au nucleation temperature, as shown by the red dot. "L" denotes liquid.

can lower the Au nucleation temperature by roughly 40 K, and a 4% increase in Ge might stabilize the liquid phase against Au nucleation at temperatures as low as 260°C. Such large kinetically driven supersaturations are not expected in typical macroscopic systems but become increasingly likely in strongly facetted systems as they shrink to the nanoscale (*28*, *31*). The degree of supersaturation would increase with growth rate, which could explain the successful growth of Ge nanowires at temperatures as low as 260°C in conventional chemical vapor deposition, where the growth rate is far higher than that in our experiments.

In conclusion, we have shown that during the growth of Ge wires using Au, the catalyst state may be either solid or liquid below T_e, with the state depending not just on temperature but also on Ge_2H_6 pressure and history. Nanowire growth continues regardless of the state the catalyst is in. In other words, both VLS and VSS processes can operate under the same conditions to grow Ge wires. A substantial Ge_2H_6 pressure is essential for growth via VLS below T_e. We propose a possible mechanism for the existence of a liquid catalyst at these temperatures, which is consistent with the observed dependence on Ge_2H_6 pressure and wire diameter. These results demonstrate that source gas pressure, though generally not considered a key factor, is actually crucial in determining the growth mode. The role of growth pressure and history may be relevant to controlling nanowire synthesis below T_e and to resolving the controversy surrounding the catalyst state in other materials systems.

References and Notes

1. K. Haraguchi, T. Katsuyama, K. Hiruma, K. Ogawa, *Appl. Phys. Lett.* **60**, 745 (1992).
2. J. Hu, T. W. Odom, C. M. Lieber, *Acc. Chem. Res.* **32**, 435 (1999).
3. L. Samuelson, *Mater. Today* **6**, 22 (2003).
4. H. J. Fan, P. Werner, M. Zacharias, *Small* **2**, 700 (2006).
5. R. S. Wagner, W. C. Ellis, *Appl. Phys. Lett.* **4**, 89 (1964).
6. Y. Wang, V. Schmidt, S. Senz, U. Gösele, *Nat. Nanotechnol.* **1**, 186 (2006).
7. Y. Yao, S. Fan, *Mater. Lett.* **61**, 177 (2007).
8. T. I. Kamins, R. S. Williams, D. P. Basile, T. Hesjedal, J. S. Harris, *J. Appl. Phys.* **89**, 1008 (2001).
9. G. A. Bootsma, H. J. Gassen, *J. Cryst. Growth* **10**, 223 (1971).
10. Y. Miyamoto, M. Hirata, *Jpn. J. Appl. Phys.* **14**, 1419 (1975).
11. D. Wang, H. Dai, *Angew. Chem. Int. Ed.* **41**, 4783 (2002).
12. T. I. Kamins, X. Li, R. S. Williams, *Nano Lett.* **4**, 503 (2004).
13. A. B. Greytak, L. J. Lauhon, M. S. Gudiksen, C. M. Lieber, *Appl. Phys. Lett.* **84**, 4176 (2004).
14. H. Adhikari, A. F. Marshall, C. E. D. Chidsey, P. C. McIntyre, *Nano Lett.* **6**, 318 (2006).
15. K. Hiruma *et al.*, *J. Appl. Phys.* **77**, 447 (1995).
16. A. I. Persson *et al.*, *Nat. Mater.* **3**, 677 (2004).
17. J. C. Harmand *et al.*, *Appl. Phys. Lett.* **87**, 203101 (2005).
18. M. Tchernycheva, J. C. Harmand, G. Patriarche, L. Travers, G. E. Cirlin, *Nanotechnology* **17**, 4025 (2006).
19. K. A. Dick *et al.*, *Nano Lett.* **5**, 761 (2005).
20. H. D. Park, A.-C. Gaillot, S. M. Prokes, R. C. Cammarata, *J. Cryst. Growth* **296**, 159 (2006).
21. S. Kodambaka, J. Tersoff, M. C. Reuter, F. M. Ross, *Phys. Rev. Lett.* **96**, 096105 (2006).
22. O. G. Shpyrko *et al.*, *Science* **313**, 77 (2006).
23. Q. Xu *et al.*, *Phys. Rev. Lett.* **97**, 155701 (2006).
24. F. M. Ross, J. Tersoff, M. C. Reuter, *Phys. Rev. Lett.* **95**, 146104 (2005).
25. F. Glas, J.-C. Harmand, *Phys. Rev. B* **73**, 155320 (2006).
26. Using 160 kJ/mol for the heat of reaction $Ge_2H_6 \rightarrow 2Ge + 3H_2$ (*32*) and a thermal conductivity of 5 W/mK for a 20-nm-wide wire, and assuming that all heat is conducted away, we estimate a maximum temperature difference ΔT of $\sim 10^{-5}$ K between the base and the tip of a 1-μm-long wire growing at 10^{-5} Torr of Ge_2H_6. In case of heat loss through radiation to the ambient, $\Delta T \sim 10^{-2}$ K.
27. N. Mingo, L. Yang, D. Li, A. Majumdar, *Nano Lett.* **3**, 1713 (2003).
28. S. D. Peteves, R. Abbaschian, *Metall. Trans. A* **22A**, 1259 (1991).
29. T. B. Massalski, J. L. Murray, L. H. Bennett, H. Baker, Eds. *Binary Alloy Phase Diagrams* (American Society for Metals, Metals Park, OH, 1986), vol. 1, pp. 263–264.
30. J. L. Taraci *et al.*, *Appl. Phys. Lett.* **84**, 5302 (2004).
31. M. J. Aziz, in *The Selected Works of John W. Cahn*, W. C. Carter, W. C. Johnson, Eds. (Minerals, Metals, and Materials Society, Warrendale, PA, 1998), pp. 207–209.
32. D. R. Lide, Ed., *CRC Handbook of Chemistry and Physics* (CRC Press, Boca Raton, FL, 2005).

33. We acknowledge R. M. Tromp, S. Guha, M. A. Aziz, and E. Tutuc for helpful discussions; A. Ellis for the development of in situ microscopy facilities; and L. Gignac and K. B. Reuter for energy-dispersive x-ray and electron energy-loss spectroscopy analyses of the wires. This work was partially supported by Defense Advanced Research Projects Agency (DARPA) under contract N66001-05-C-6030.

Supporting Online Material

www.sciencemag.org/cgi/content/full/316/5825/729/DC1
Fig. S1

20 December 2006; accepted 21 March 2007
10.1126/science.1139105

Synthesis of Tetrahexahedral Platinum Nanocrystals with High-Index Facets and High Electro-Oxidation Activity

Na Tian,[1] Zhi-You Zhou,[1] Shi-Gang Sun,[1]* Yong Ding,[2] Zhong Lin Wang[2]*

The shapes of noble metal nanocrystals (NCs) are usually defined by polyhedra that are enclosed by {111} and {100} facets, such as cubes, tetrahedra, and octahedra. Platinum NCs of unusual tetrahexahedral (THH) shape were prepared at high yield by an electrochemical treatment of Pt nanospheres supported on glassy carbon by a square-wave potential. The single-crystal THH NC is enclosed by 24 high-index facets such as {730}, {210}, and/or {520} surfaces that have a large density of atomic steps and dangling bonds. These high-energy surfaces are stable thermally (to 800°C) and chemically and exhibit much enhanced (up to 400%) catalytic activity for equivalent Pt surface areas for electro-oxidation of small organic fuels such as formic acid and ethanol.

Generally, catalytic performance of nanocrystals (NCs) can be finely tuned either by their composition, which mediates electronic structure (*1*, *2*), or by their shape, which determines surface atomic arrangement and coordination (*3*, *4*). Fundamental studies of single-crystal surfaces of bulk Pt have shown that high-index planes generally exhibit much higher catalytic activity than that of the most common stable planes, such as {111}, {100}, and even {110}, because the high-index planes have a high density of atomic steps, ledges, and kinks, which usually serve as active sites for breaking chemical bonds (*5*–*7*). For example, a bulk Pt(210) surface possesses extremely high catalytic reactivity for electroreduction of CO_2 (*8*) and electro-oxidation of formic acid (*9*). The bulk Pt(410) surface exhibits unusual activity for catalytic decomposition of NO, a major pollutant of automobile exhaust (*10*). Thus, the shape-controlled synthesis of metal NCs bounded by high-index facets is a potential route for enhancing their catalytic activities.

It is, however, rather challenging to synthesize shape-controlled NCs that are enclosed by high-index facets because of their high surface energy. Crystal growth rates in the direction perpendicular to a high-index plane are usually much faster than those along the normal direction of a low-index plane, so high-index planes are rapidly eliminated during particle formation (*11*). During the past decade, a variety of face-centered cubic (fcc) structured metal NCs with well-defined shapes have been synthesized, but nearly all of them are bounded by the low-index planes, such as tetrahedron, octahedron, decahedron, and icosahedron, enclosed by {111} facets (*12*–*14*), cube by {100} (*12*, *15*), cuboctahedron by {111} and {100} (*16*), and rhombic dodecahedron by {111} (*17*). Here we describe an electrochemical method for the synthesis of tetrahexahedral (THH) Pt NCs at high purity. The THH shape is bounded by 24 facets of high-index planes ~{730} and vicinal planes such as {210}

[1]State Key Laboratory of Physical Chemistry of Solid Surfaces, Department of Chemistry, College of Chemistry and Chemical Engineering, Xiamen University, Xiamen 361005, China. [2]School of Materials Science and Engineering, Georgia Institute of Technology, Atlanta, GA 30332–0245, USA.

*To whom correspondence should be addressed. E-mail: sgsun@xmu.edu.cn (S.G.S.); zhong.wang@mse.gatech.edu (Z.L.W.)